ECS The Electrochemical Society
Advancing solid state & electrochemical science & technology

Three-Dimensional Self-Ordered Multilayered Ge Nanodots on SiGe

View the article online for updates and enhancements.

Three-Dimensional Self-Ordered Multilayered Ge Nanodots on SiGe

Wei-Chen Wen,[1,z] Markus Andreas Schubert,[1] Marvin Hartwig Zoellner,[1] Bernd Tillack,[1,2] and Yuji Yamamoto[1]

[1]*IHP - Leibniz-Institut für innovative Mikroelektronik, Im Technologiepark 25, Frankfurt (Oder) 15236, Germany*
[2]*Technische Universität Berlin, HFT4, Einsteinufer 25, Berlin 10587, Germany*

Three-dimensional (3D) self-ordered Ge nanodots in cyclic epitaxial growth of Ge/SiGe superlattice on $Si_{0.4}Ge_{0.6}$ virtual substrate (VS) were fabricated by reduced pressure chemical vapor deposition. The Ge nanodots were formed by Stranski-Krastanov mechanism. By the Ge/SiGe superlattice deposition, dot-on-dot alignment and $\langle 100 \rangle$ alignment were obtained toward the vertical and lateral direction, respectively. Facets and growth mechanism of Ge nanodots and key factors of alignment were studied. Two types of Ge nanodots were observed, diamond-like nanodots composed of {105} and dome-like nanodots composed of {113} and {519} or {15 3 23} facets. The Ge nanodots tend to grow directly above the nanodots of the previous period as these regions show a relatively higher tensile strain induced by the buried nanodots. Thus, this dot-on-dot alignment is sensitive to the SiGe spacer thickness, and it degrades when the SiGe spacer becomes thicker. The Ge content of the SiGe spacer ranging from 45 to 52% affects the lateral alignment and the size uniformity of Ge nanodots because of the strain balance between the superlattice and the VS. By maintaining the strain balance, ordering of the 3D aligned Ge nanodots can be improved.

Ge nanodots have drawn much attention due to their potential applications in optoelectronics, such as photodetectors and lasers.[1–10] Many groups studied multilayered Ge nanodots with Si spacers on Si(001) grown by Stranski-Krastanov (SK) growth mode and vertically aligned by local tensile strain induced by buried Ge nanodots.[11–17] However, to avoid plastic relaxation caused by a 4.2% lattice mismatch between Si and Ge, thick nanodots and/or large layer numbers are challenging. Even though the vertical alignment of the Ge nanodots is realized, the Ge nanodots are randomly distributed in lateral direction. In order to fabricate laterally-ordered Ge nanodots, pre-structuring is required.[12,15]

Vertical and lateral alignment of SiGe nanodots with Si spacers on Si substrate were reported, and the elastic anisotropy of the spacer material is the key to the lateral alignment.[18,19] To predict and to control the surface density and size distribution of nanodots, nucleation and growth behavior around existing nanodot were simulated,[20] and elastic interactions between nanodots on the growth behavior were reported.[21–23] In our previous work, laterally and vertically self-aligned multilayered SiGe nanodots fabrication with Si spacer on Si(001) were studied.[24,25] Vertical and body-centered-tetragonal alignment were obtained by controlling local distribution and surface energy. In this study, we demonstrate 3-dimensional (3D) self-ordered Ge nanodots on SiGe virtual substrate (VS) by SiGe/Ge cyclic epitaxial growth and discuss the effects of fabrication parameters. The facets of Ge nanodots and the mechanism of vertical alignment are also studied.

Experimental

The 3D self-ordered Ge epitaxial nanodots were fabricated by reduced-pressure chemical vapor deposition (RPCVD). Firstly, a $Si_{0.4}Ge_{0.6}$ VS with step-graded buffer on on-oriented Si(001) wafer (with ~0.16° slice off orientation on average) was fabricated to reduce dislocation density and mosaicity of crystal compared to conventional single box VS. In order to realize high quality VS, cyclic annealing at 1000 °C was carried out after each step-graded layer deposition to achieve fully relaxed layers and to improve crystallinity of each layer. By the cyclic annealing at 1000 °C, additional ~0.1% tensile strain is introduced in the $Si_{0.4}Ge_{0.6}$ VS due to thermal expansion coefficient difference between Si and

SiGe, which was confirmed by X-ray diffraction (XRD) reciprocal space mapping (RSM). Furthermore, ~2 μm thick $Si_{0.4}Ge_{0.6}$ was deposited followed by postannealing at 1000 °C. Afterwards chemical mechanical polishing was performed to obtain a smooth surface. The dislocation density of 1×10^7 cm^{-2} was confirmed by Secco defect etching followed by pit count on an angle view SEM image. After HF dip, the wafer was baked at 850 °C in H_2 to remove residual oxide and then cooled down to 550 °C for epitaxial growth. A 52–82 nm thick layer of SiGe with 45%–52% Ge content was deposited using a H_2-SiH_4-GeH_4 gas mixture (deposition rate: approximately 29–33 nm min^{-1}), then a self-assembled Ge nanodots layer via SK growth mechanism was deposited with equivalent Ge thickness of 7.5–15.0 nm using a H_2-GeH_4 gas mixture (deposition rate: approximately 19 nm min^{-1}). This SiGe/Ge deposition cycle was repeated 5 to 20 times to fabricate the 3D self-ordered Ge nanodot stack. The superlattice of 12.5 nm-Ge/52 nm-$Si_{0.48}Ge_{0.52}$ was used as a standard because the weighted average lattice constant is nearly the same as the $Si_{0.4}Ge_{0.6}$ VS. The composition of SiGe VS and SiGe spacers were confirmed by XRD RSM and XRD, respectively.[26]

Atomic force microscopy (AFM) was used to analyze the morphology and alignment of the Ge nanodots. Scanning electron microscopy (SEM) with energy selective backscatter detector and in-lens detector was used to investigate the vertical- and lateral alignments of the Ge nanodots, respectively. The facets of the Ge nanodots were studied by analyzing the cross-section cuts of AFM images and confirmed by scanning transmission electron microscopy (STEM). Grazing incidence in-plane XRD (GIXRD) and STEM-based Nano-beam diffraction (NBD) were used to study strain in the superlattice and the mechanism of vertical alignment.

Results and Discussion

In order to optimize vertical and lateral alignment of the Ge nanodot, several growth parameters, such as thickness of Ge and SiGe spacer, Ge content of SiGe spacer and cycle number of the superlattice, were adjusted, and their influence on the morphology and alignment of Ge nanodots were studied. Facets of Ge nanodots were investigated, and strain distribution and mechanism of vertical alignment were discussed.

Morphology of Ge nanodots.—Figures 1a–1d show an angle view SEM image and AFM images of Ge nanodots on the 5-cycle

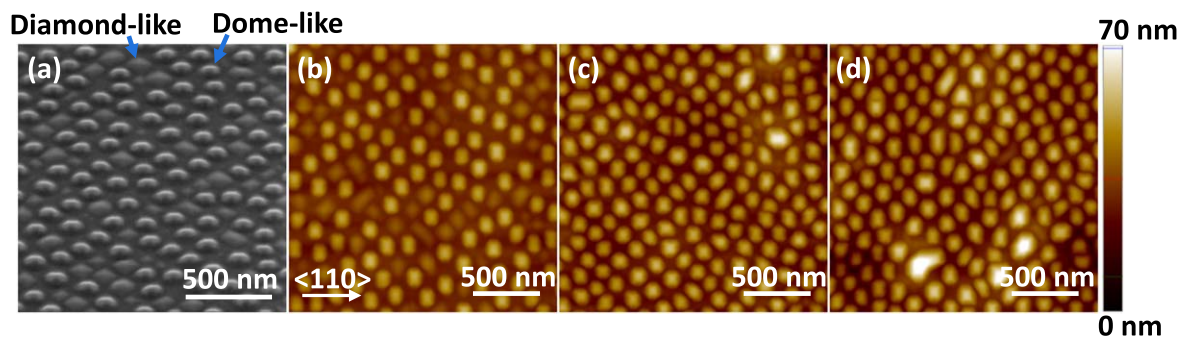[z]E-mail: wei-chen.wen@ihp-microelectronics.com

Figure 1. (a) An angle view of SEM image (view at an angle of 40° to the surface) of Ge nanodots on 5-cycle superlattice of 7.5 nm-Ge/52 nm-SiGe and AFM images of Ge nanodots on 5-cycle superlattice of (b) 7.5 nm-Ge/52 nm-SiGe (c) 12.5 nm-Ge/52 nm-SiGe and (d) 15.0 nm-Ge/52 nm-SiGe superlattice. The Ge content of SiGe spacer is 52%.

superlattices with Ge thickness of 7.5 to 15.0 nm. The Ge nanodots align diagonally (along $\langle 100 \rangle$), which can be clearly confirmed in the later discussion. In Figs. 1a–1b, mainly two types of nanodots are observed, which are diamond (32%) and dome (68%) like shape. Figure 2 shows the height distribution of diamond-like and dome-like nanodots appearing in Fig. 1b. The average height of the diamond-like nanodots is approximately 9 nm with a standard deviation (s) of 2.6 nm while that of the dome-like nanodots is approximately 23 nm with s = 1.8 nm. With increasing Ge thickness, dome-like nanodots dominate (Fig. 1c) and some nanodots merge with the adjacent nanodots (Fig. 1d). Since the dome-like nanodots show a lower s in height than the diamond-like nanodots do, as shown in Fig. 2, engineering of self-ordering is more feasible with the dome-like nanodot.

Vertical and lateral alignment of Ge nanodots.—Figures 3a–3c show the cross-section SEM images and AFM images of 5-cycle Ge/SiGe superlattice with Ge thickness of 12.5 nm and $Si_{0.48}Ge_{0.52}$ spacer thickness of 52 nm and 82 nm. The Fourier transform (FT) images of 10 μm × 10 μm AFM images, which provide the information of lateral ordering of nanodots, are shown in Figs. 3d–3e. The surface is smooth after 52 nm or 82 nm $Si_{0.48}Ge_{0.52}$ spacer deposition (Figs. 3a–3b), implying the adequate surface reaction and atom migration to form a stabilized (001) surface. When the 52 nm SiGe spacer was used, dot-on-dot alignment with Ge wetting layer can be observed (Fig. 3a). This vertical alignment is because the Ge nanodots prefer to grow in the region with lateral tensile strain induced by the buried Ge nanodots. The details will be discussed later. When the thickness of $Si_{0.48}Ge_{0.52}$ spacer increases, the vertical alignment of Ge nanodots becomes relatively random (Fig. 3b), the size and the shape of Ge nanodots become irregular, and some diamond-like nanodots appear (Fig. 3c). This is related to the reduced local tensile strain caused by the increased distance of the buried Ge nanodots. The less strain difference over the SiGe surface appears the less driving force which affects the vertical alignment for dome-like nanodot formation. Besides, the lateral alignment of Ge nanodots degrades, which can be confirmed from the FT image as shown in Figs. 3d–3e. Diagonal alignment (along $\langle 100 \rangle$ direction, which is elastically soft direction) with a period of approximately 157 nm can be confirmed in the strain-balanced superlattice (Fig. 3d). The mechanism of self-ordering may be similar to SiGe island chains on Si substrate.[27] However, for the superlattice with 82 nm SiGe spacer, the FT peaks become blurred and broad. This could also result from the less strain difference to form the Ge nanodots at specific locations. Therefore, Ge nanodot formation in each layer is like the first layer, a random SK growth. In addition, the unbalanced strain of the superlattice to the VS may also have an influence.

Figures 4a–4c show the angle view of SEM images of Ge nanodots on 5-cycle 12.5 nm-Ge/52 nm-SiGe with Ge content 52%–45%. The Ge nanodots are diagonally aligned, which can also be confirmed by the FT image in Fig. 4a. With decreasing Ge
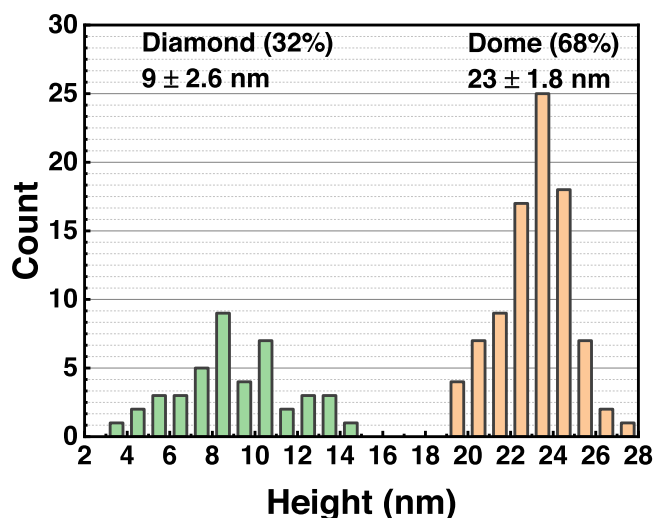

Figure 2. A height histogram of diamond-like and dome-like nanodots in Fig. 1b.

content in the SiGe spacer, large nanodots and nanodot clusters appear (Fig. 4b) and these large nanodots align along $\langle 110 \rangle$ (Fig. 4c). Because the Ge nanodots were grown on the SiGe virtual substrate, which is not as perfect as Si wafer and contains dislocations, some irregular nanodots which might be defect related can be seen in Fig. 4a. With reducing Ge concentration in the SiGe spacers, the number of these irregular nanodots becomes double and eight times as shown in Fig. 4b and in Fig. 4c, respectively. This may result from the misfit dislocation formation due to increased tensile strain in the SiGe/Ge superlattice on the $Si_{0.4}Ge_{0.6}$ VS. In addition, the lateral alignment is also influenced, and this can be seen from the FT images as shown in the insets.

Figures 5a–5c show the angle view of SEM images of Ge nanodots on 1-, 5- and 20-cycle superlattice of 12.5 nm-Ge/52 nm-SiGe. Although the nanodot size and type are not yet uniform at the first cycle, the Ge nanodots are to some degree laterally aligned, which can be seen in the FT image (Fig. 5a). With the cycle number increasing, the dome-like nanodots are dominant and the lateral alignment is easily seen. The greater the layer number, the better the starting point in terms of alignment and uniformity for Ge nanodot formation. Accordingly, the alignment and the uniformity of nanodot shape and size improve with the increasing cycle number of the superlattice.

Facets of Ge nanodots.—To study facets of two types of nanodots, the tilt of each facet was calculated from the cross-section cuts of AFM images. Figure 6 (a) shows an AFM image of the dome-like nanodot. Figure 6b shows the cross-section cuts of Fig. 6a
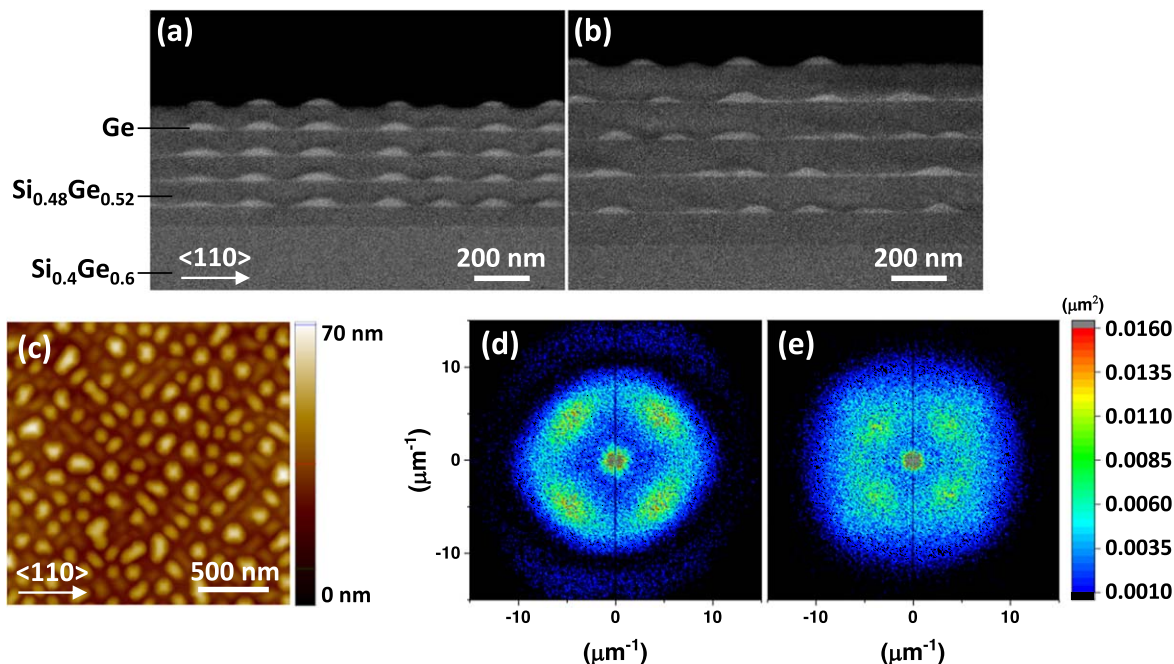
Figure 3. Cross-section SEM image of 5-cycle (a) 12.5 nm-Ge/52 nm-SiGe and (b) 12.5 nm-Ge/82 nm-SiGe superlattice, (c) AFM images of Ge nanodots on 5-cycle 12.5 nm-Ge/82 nm-SiGe superlattice, and FT images of a 10 μm × 10 μm AFM images of Ge nanodots on 5-cycle (d) 12.5 nm-Ge/52 nm-SiGe and (e) 12.5 nm-Ge/82 nm-SiGe superlattice.
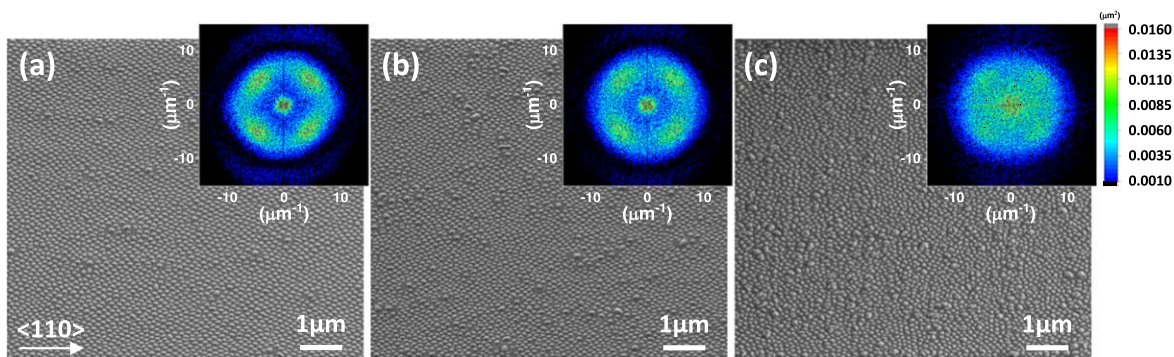

Figure 4. Angle view of SEM images (view at an angle of 40° to the surface) of Ge nanodots on 5-cycle superlattice of 12.5 nm-Ge/52 nm-SiGe with Ge content (a) 52% (b) 49% and (c) 45% on $Si_{0.4}Ge_{0.6}$ VS. The insets are the FT images of 10 μm × 10 μm AFM images of corresponding samples.
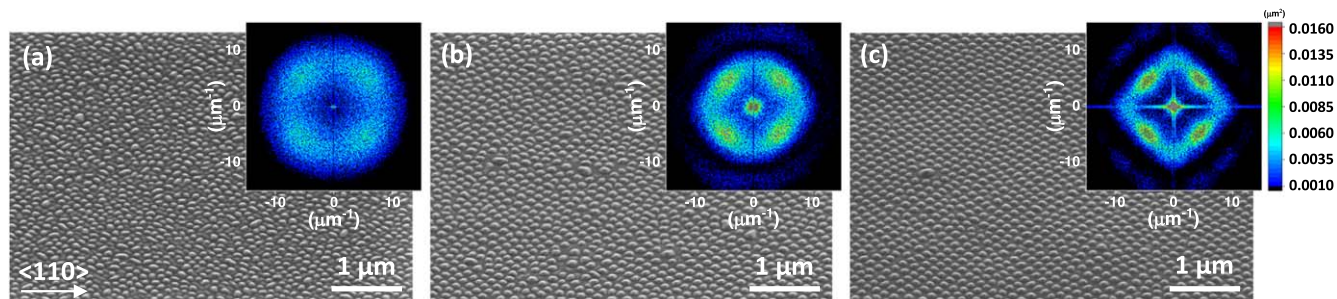

Figure 5. Angle view of SEM images (view at an angle of 40° to the surface) of Ge nanodots on (a) 1-cycle, (b) 5-cycle and (c) 20-cycle superlattice of 12.5 nm-Ge/52 nm-SiGe with 52% Ge content.

along ⟨110⟩. These cross-section cuts are well-overlapped with the high-angle annular dark-field (HAADF) STEM image as shown in the background of Fig. 6b. Therefore, it is possible and reliable to estimate the facets from the cross-section cuts of our AFM images. For example, the side wall of the dome-like Ge nanodot in Fig. 6b is approximately 25°, indicating {113} facets. Similarly, an AFM

image of the diamond-like Ge nanodot and cross-section cuts along ⟨110⟩ were shown in Figs. 6c and 6d, respectively. These cross-section curves are nearly parallel to each other on the side, indicating two facets on both sides. According to the angle of the side wall, 8°, it suggests {105} facets. By this method, we confirmed that the diamond-like nanodot is composed of {105} and the dome-like
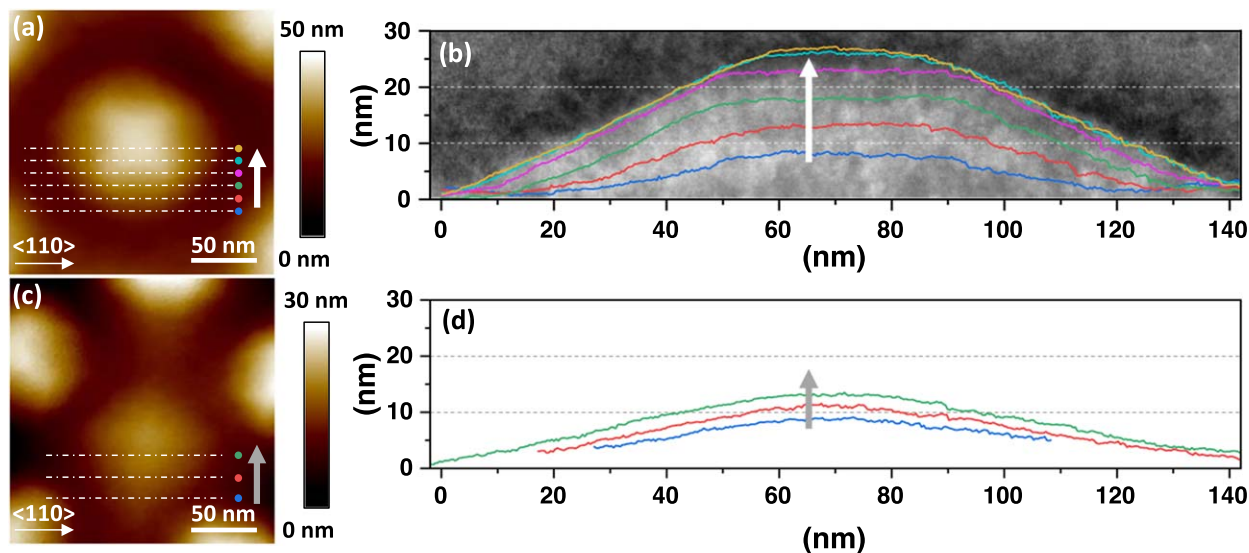
Figure 6. (a) AFM image and (b) cross-section cuts (along ⟨110⟩) of the AFM image overlapped with HAADF STEM image of dome-like Ge nanodot and (c) AFM image and (d) cross-section cuts (along ⟨110⟩) of the AFM of diamond-like Ge nanodot. The Ge nanodots are on top of 20-cycle superlattice of 12.5 nm-Ge/52 nm-SiGe. The Ge content of the SiGe spacer is 52%.
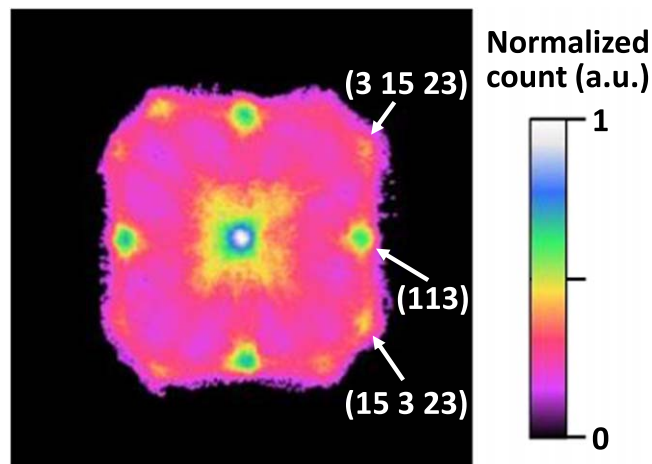

Figure 7. Stereographic map around (001) pole of a 500×500 nm^2 AFM image of Ge nanodots on top of 20-cycle superlattice of 12.5 nm-Ge/52 nm-SiGe.

Figure 8. In-plane XRD of 52 nm-SiGe, 12.5 nm-Ge/52 nm-SiGe and 52 nm-SiGe/12.5 nm-Ge/52 nm-SiGe on $Si_{0.4}Ge_{0.6}$ VS. The Ge content of the SiGe spacer is 52%. Here, the angle of incidence is the critical angle of 0.23° and the penetration depth is approximately 60 nm. As a reference, the $2\theta\chi$ of a non-strained Ge, $Si_{0.4}Ge_{0.6}$ and $Si_{0.48}Ge_{0.52}$ are marked in the figure.

nanodot is composed of {113} and {519} facets. This is consistent with the studies of Ge dot on Si substrate except for {519} facets. Instead of {519} facets, relatively similar {15 3 23} facets were reported.[28,29] This difference is thought to be the less compressive strain in our Ge nanodots because a SiGe VS was used and/or measurement error due to the algorism of AFM image leveling.

In order to confirm the facet of the dome-like Ge nanodots, a wider area range of Ge nanodots was investigated with a similar method to Refs. 28, 29. Figure 7 shows the quantitative facet analysis of dome-like nanodots in a 500×500 nm^2 AFM image. This stereographic map provides the facet angular orientation and the facet inclination with respect to the (001) surface, and the color gradient indicates the normalized count of facets. The central spot is the (001) plane corresponding to the wetting layer and the top of Ge nanodots. The other two groups of spots with two different radiuses in the stereographic map, indicating the polar angle of 25.2° and 33.6°, correspond to {113} and {15 3 23} facets, respectively. The azimuthal angles of these facets with respect to the [110] direction are 0° and 33.7°, respectively. The reason that we obtained {519} facets and {15 3 23} facets by different
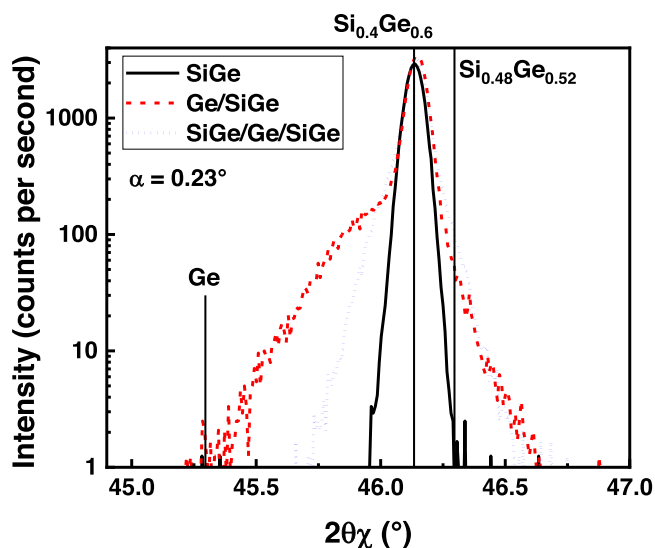
analysis methods could be the background leveling of AFM images with different area sizes and different numbers of nanodots.

Strain distribution and mechanism of vertical alignment.—To explain the vertical correlation of Ge nanodots, strain evolution during superlattice growth and strain distribution were studied by XRD and NBD, respectively. Grazing incidence in-plane XRD (220) curves of SiGe, Ge/SiGe and SiGe/Ge/SiGe on $Si_{0.4}Ge_{0.6}$ VS were measured, as shown in Fig. 8. The angle of incidence is 0.23°, corresponding to an attenuation length between 40 nm and 70 nm, for Ge and Si, respectively. For the sample with only a single layer of SiGe spacer on the VS, the peak position of 46.1° corresponds to the lateral lattice parameter of the $Si_{0.4}Ge_{0.6}$ VS, implying the SiGe spacer was pseudomorphically grown on the VS. After the Ge deposition, a broad bump can be seen at the low angle side, indicating a larger in-plane lattice parameter. This is caused by the strain relaxation as consequence
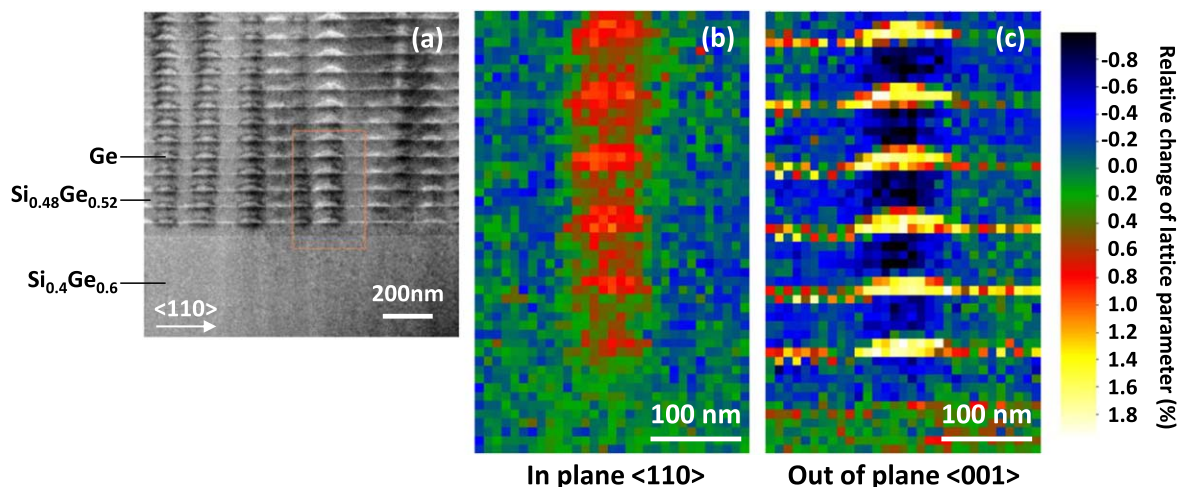
Figure 9. (a) HAADF STEM image and (b) in-plane and (c) out-of-plane relative change of lattice parameter distributions of 20-cycle superlattice of 12.5 nm-Ge/52 nm-SiGe. The relative change of lattice parameter was measured by NBD, and the reference parameter (0% change) was taken at $Si_{0.4}Ge_{0.6}$ VS.

upon Ge nanodot formation. After second SiGe spacer deposition the curve is nearly symmetric but broader. This implies that the SiGe spacer above Ge nanodots may have a larger lateral lattice parameter distribution which is responsible for the dot-on-dot alignment. As the peak has also no shift or bump compared to the Ge/SiGe curve, the strain relaxation in the Ge nanodots is most probably of elastic nature. This means that the lateral lattice parameter of Ge nanodots may be compressed by the SiGe on top, suggesting that the SiGe/Ge/SiGe is pseudomorphically grown on the VS.

A HAADF STEM image and in- and out-of-plane relative change of lattice parameter distributions measured by NBD are shown in Figs. 9a –9c. The nanodots are vertically aligned, and the wetting layer of Ge is approximately 2 nm regardless of the layer number (Fig. 9a). The SiGe on the nanodot shows a relatively higher lattice parameter along ⟨110⟩ (Fig. 9b) and lower lattice parameter along ⟨001⟩ (Fig. 9c) compared to that on Ge wetting layer, indicating tensile strain. These results support the discussion on strain distribution measured by in-plane XRD. When the surface of SiGe spacer is smooth, the tensile strain area is the preferred position for Ge nanodot formation because of less lateral lattice mismatch. Consequently, the nanodots tend to grow above the buried nanodots. On the other hand, if the SiGe spacer is too thick, the strain at the SiGe surface becomes uniform, thus causing a random Ge nanodot formation as shown in Figs. 3b–3c.

Conclusions

3D self-ordered multilayered Ge nanodots on SiGe VS were fabricated using RPCVD. The Ge nanodots were vertically aligned on the nanodot and laterally aligned along ⟨100⟩ in the Ge/SiGe superlattice. Diamond-like Ge nanodots composed of {105} facets and dome-like nanodots composed of {113} and {519} or {15 3 23} facets were observed. To unify the shape of the Ge nanodots, Ge thickness is the key parameter. By increasing the thickness of Ge from 7.5 nm to 12.5 nm, the morphology of Ge nanodots changed from a mixture of diamond-like and dome-like to mainly dome-like. When the thickness of Ge further increased to 15 nm, some nanodots merged with other nanodots in the vicinity. The mechanism of dot-on-dot vertical alignment is that the Ge nanodots tend to grow at the region on the Ge nanodots with the lateral tensile strain induced by the buried Ge nanodots. Therefore, the thick SiGe spacer (82 nm) degrades the vertical alignment due to the insufficient tensile strain difference on the SiGe surface with increasing distance. In addition to the Ge thickness and SiGe thickness, the Ge content of SiGe spacer and the cycle number of superlattice also affect the size uniformity and the lateral alignment of Ge nanodots because a strain-balanced superlattice is required for the continuously aligned Ge nanodots formation.

Growing large layer number of 3D aligned Ge nanodots can be possible when the layer stacks are strain balanced to the VS.

ORCID

Wei-Chen Wen https://orcid.org/0000-0001-6804-9562
Yuji Yamamoto https://orcid.org/0000-0003-0928-4356

References

1. M. Brehm and M. Grydlik, *Nanotechnology*, **28**, 392001 (2017).
2. K. Makihara, M. Ikeda, N. Fujimura, K. Yamada, A. Ohta, and S. Miyazaki, *Appl. Phys. Express*, **11**, 11305 (2017).
3. X. Xu, N. Usami, T. Maruizumi, and Y. Shiraki, *J. Cryst. Growth*, **378**, 636 (2013).
4. B.-C. Hsu, S. T. Chang, T.-C. Chen, P.-S. Kuo, P. S. Chen, Z. Pei, and C. W. Liu, *IEEE Electron Device Lett.*, **24**, 318 (2003).
5. J. W. John, V. Dhyani, S. Singh, A. Jakhar, A. Sarkar, S. Das, and S. K. Ray, *Nanotechnology*, **32**, 315205 (2021).
6. S. Shi, D. Pacifici, and A. Zaslavsky, *Appl. Phys. Lett.*, **119**, 221108 (2021).
7. S. Cosentino et al., *Appl. Phys. Lett.*, **98**, 221107 (2011).
8. Q. Chen et al., *ACS Appl. Nano Mater.*, **4**, 897 (2021).
9. P. Krause, J. C. Tremblay, and A. Bande, *J. Phys. Chem.*, **125**, 4793 (2021).
10. M. Grydlik, F. Hackl, H. Groiss, M. Glaser, A. Halilovic, T. Fromherz, W. Jantsch, F. Schäffler, and M. Brehm, *ACS photonics*, **3**, 298 (2016).
11. M. S. Storozhevykh, L. V. Arapkina, S. M. Novikov, V. S. Volkov, A. V. Arsenin, O. V. Uvarov, and V. A. Yuryev, *J Raman Spectroscopy*, **53**, 853 (2022).
12. K. L. Wang, D. Cha, J. Liu, and C. Chen, *Proceedings of the IEEE* **95**, 1866 (2007).
13. P. S. Chen, Z. Pei, Y. H. Peng, S. W. Lee, and M.-J. Tsai, *Materials Science and Engineering:*, **108**, 213 (2004).
14. A. Alguno, N. Usami, T. Ujihara, K. Fujiwara, G. Sazaki, K. Nakajima, and Y. Shiraki, *Appl. Phys. Lett.*, **83**, 1258 (2003).
15. O. G. Schmidt and K. Eberl, *IEEE Trans. Electron Devices*, **48**, 1175 (2001).
16. V. Le Thanh, V. Yam, Y. Zheng, and D. Bouchier, *Thin Solid Films*, **380**, 2 (2000).
17. Y. Yamamoto, Y. Itoh, P. Zaumseil, M. A. Schubert, G. Capellini, K. Washio, and B. Tillack, *ECS J. Solid State Sci. Technol.*, **8**, P190 (2019).
18. C. Teichert, M. G. Lagally, L. J. Peticolas, J. C. Bean, and J. Tersoff, *Phys. Rev.*, **53**, 16334 (1996).
19. G. Springholz, M. Pinczolits, V. Holy, S. Zerlauth, I. Vavra, and G. Bauer, *Physica E*, **9**, 149 (2001).
20. K. Liu, I. Berbezier, L. Favre, A. Ronda, M. Abbarchi, P. Donnadieu, P. W. Voorhees, and J.-N. Aqua, *Nanoscale*, **11**, 7798 (2019).
21. V. A. Shchukin, D. Bimberg, T. P. Munt, and D. E. Jesson, *Phys. Rev.*, **70**, 85416 (2004).
22. F. Montalenti, A. Marzegalli, G. Capellini, M. D. Seta, and L. Miglio, *J. Phys. Condens. Matter*, **19**, 225001 (2007).
23. I. I. Izhnin, O. I. Fitsych, A. V. Voitsekhovskii, A. P. Kokhanenko, K. A. Lozovoy, and V. V. Dirko, *Appl. Nanosci.*, **10**, 2527 (2020).
24. Y. Yamamoto, P. Zaumseil, G. Capellini, M. Andreas Schubert, A. Hesse, M. Albani, R. Bergamaschini, F. Montalenti, T. Schroeder, and B. Tillack, *Nanotechnology*, **28**, 485303 (2017).
25. Y. Yamamoto, Y. Itoh, P. Zaumseil, M. A. Schubert, G. Capellini, F. Montalenti, K. Washio, and B. Tillack, *Semicond. Sci. Technol.*, **33**, 114014 (2018).
26. J. P. Dismukes, L. Ekstrom, and R. J. Paff, *J. Phys. Chem.*, **68**, 3021 (1964).
27. M. Meixner, E. Schöll, M. Schmidbauer, H. Raidt, and R. Köhler, *Phys. Rev.*, **64**, 797 (2001).
28. J. T. Robinson, A. Rastelli, O. Schmidt, and O. D. Dubon, *Nanotechnology*, **20**, 85708 (2009).
29. A. Rastelli and H. von Känel, *Surf. Sci.*, **515**, L493 (2002).